XII SEPOPE
20 a 23 de Maio 2012
May – 20th to 23rd – 2012
RIO DE JANEIRO (RJ) - BRASIL

XII SIMPÓSIO DE ESPECIALISTAS EM PLANEJAMENTO DA OPERAÇÃO E EXPANSÃO ELÉTRICA

XII SYMPOSIUM OF SPECIALISTS IN ELECTRICAL OPERATION AND EXPANSION PLANNING

Security-Constrained Optimal Power Flow including Post-Contingency Control of VSC-HVDC lines

Spyros CHATZIVASILEIADIS, Thilo KRAUSE, Göran ANDERSSON

ETH Zurich

Switzerland

SUMMARY

The paper proposes a security-constrained optimal power flow algorithm (SC-OPF) which allows the post-contingency control of High Voltage Direct Current lines, based on the Voltage Source technology (VSC-HVDC). The presented algorithm integrates corrective actions of HVDC lines in a single optimization problem, without the need to solve a detailed power flow or OPF for each contingency. The approach is based on the current injection method, which is extended to include the HVDC control actions during the post-fault line flow calculation. The algorithm determines the active and reactive power injections (resp. withdrawals) in order to alleviate line overloads and meet post-contingency voltage setpoints. One additional optimization variable is added for each HVDC line and critical contingency considered.

The proposed approach can be used for both power system operation and planning. For planning studies with focus on system security, the term 'Cost of Security' is introduced. The 'Cost of Security' provides a quantitative index for evaluating expansion scenarios with respect to the additional cost incurred in order to fulfill the N-1 security criterion. The most attractive solution should result in the least 'Cost of Security'.

The proposed algorithm is applied to three case studies in order to test its performance. The last case study deals with a single-node per country European power system model, based on real data, which represents the cross-border flows. Control actions for multiple HVDC lines, considering several critical contingencies, are presented.

KEYWORDS

corrective control, Cost of Security, N-1 security criterion, current injection method, Voltage-Source Converters, High Voltage Direct Current

e-mail: spyros@eeh.ee.ethz.ch; address: Physikstrasse 3, CH-8092 Zurich; tel:+41 44 632 8990

1. Introduction

Worldwide, power systems experience a paradigm change. Increased environmental awareness and market developments lead to resource-dependent power infeed and increased cross-border power flows. It has become obvious that the need for investments in power transmission infrastructure is growing, not only for replacing aging grid assets but also in order to extend the grid capabilities, taking advantage of technology developments. High Voltage Direct Current systems are expected to play a key role in transmission reinforcement projects, as they allow the transfer of power over longer distances with lower losses and enhance the controllability of the power system. Projects such as the off-shore grid in the North Sea (www.offshoregrid.eu), or Desertec (www.desertec.org) suggest the interconnection through HVDC lines.

HVDC systems based on the Voltage-Source Converter (VSC) technology, which started to be deployed during the last decade, exhibit significant flexibility as they can control independently the active and reactive power. Such systems can prove helpful in the maintenance of power system security. Due to their fast response, they are able to undertake corrective control actions in order to relieve overloads and prevent voltage drops in case of contingency [1]. Although a significant amount of literature exists for including HVDC lines in power flow and Optimal Power Flow (OPF) problems (e.g. [2], [3]), only few publications deal with security considerations, in the presence of HVDC lines. In [4], a corrective control algorithm for FACTS devices (UPFC), based on OPF, is presented. The algorithm is based on linear sensitivities and focusses more on short computation times and on finding a feasible solution, with optimality being a secondary objective. In [5], a security-constrained unit commitment including HVDC lines is presented. The problem is solved through sequential linear programming, determining the committed units and solving optimization subproblems for the base case and each contingency.

The contributions of this paper are a Security-Constrained Optimal Power Flow (SC-OPF), which integrates the control capabilities of the VSC-HVDC lines in a single optimization problem, without the need to solve a detailed power flow or OPF for each contingency; further the 'Cost of Security' measure is described and used in order to evaluate future investments. The approach for including the security constraints is based on the current injection method.

The proposed algorithm can be used for both operation and planning studies. In order to evaluate prospective investments, with respect to the additional costs that are incurred in order to maintain security, the quantitative index 'Cost of Security', first introduced in [6], is described and used in the case studies.

The remainder of the paper is organized as follows: Section 2 introduces the 'Cost of Security' index. Section 3 describes the standard OPF formulation with the inclusion of VSC-HVDC lines, while Section 4 presents the current injection method and the necessary extensions in order to formulate the SC-OPF problem and account for the post-contingency control of VSC-HVDC lines. In Section 5, three case studies are examined, and Section 6 concludes.

2. Cost of Security Approach

In order to ensure security, power system operation should always fulfill the N-1 criterion. According to the ENTSO-E definition of the N-1 criterion [7], a loss of an element within the TSO's responsibility area must not endanger the security of interconnected operation and "must not lead to the triggering of an uncontrollable cascading outage propagating across the borders or having an impact outside the borders [of the TSO responsibility area]". Most power systems in practice, not only in ENTSO-E, are bound to operate in an N-1 secure state.

Common formulations of OPF-problems usually do not consider the N-1 security criterion. An optimization problem which explicitly takes into account outage events is often termed Security-Constrained Optimal Power Flow (or SC-OPF). The objective is to find a least-cost generation dispatch such that an outage of an arbitrary line or generator will not lead to overloads at any point in

the system. It is evident that the dispatch costs determined from SC-OPF calculations will be at least equal or higher than the costs determined through a "standard" OPF.

The difference in the generation dispatch costs between a "standard" OPF and an SC-OPF is what we term the 'Cost of Security' (see Eq. 1). Essentially, the 'Cost of Security' reflects the additional costs incurred to the system, so that N-1 security is ensured [6].

$$CoS = C_{SCOPF} - C_{OPF} \quad \text{Eq. 1}$$

The 'Cost of Security' (CoS) provides a quantitative index when comparing the effects of different network reinforcements on the system with respect to power system security. The solution that results in the least 'Cost of Security' guarantees, on the one hand, the secure operation of the power system, and, at the same time, it has the maximum positive effect from a societal viewpoint, as it incurs the least additional costs.

3. AC Optimal Power Flow including VSC-HVDC Lines

The formulation of the optimization problem is divided in two parts. In this section we describe the standard formulation of an AC Optimal Power Flow (OPF) and the necessary extensions in order to include the HVDC line constraints in the algorithm. In the next section we discuss how system security is incorporated in the optimal power flow resulting in a Security-Constrained OPF.

3.1. Standard AC Optimal Power Flow (AC-OPF)

The objective of the standard AC Optimal Power Flow (AC-OPF) is usually to minimize total generation costs (see Eq. 2). The AC-OPF is implemented as follows:

$$min \sum_{j=1}^{N_{gen}} C_j \left(P_{G_j}\right) \quad \text{Eq. 2}$$

subject to:

$$f(\theta, V, P, Q) = 0, \quad \text{Eq. 3}$$

$$P_{min,i} \le P_{gen,i} \le P_{max,i}, \quad \text{Eq. 4} \qquad \left|\underline{I}_{ij}(\theta, V)\right| \le I_{ij,max}, \quad \text{Eq. 5}$$

$$Q_{min,i} \le Q_{gen,i} \le Q_{max,i}, \quad \text{Eq. 6} \qquad \left|\underline{I}_{ji}(\theta, V)\right| \le I_{ji,max}, \quad \text{Eq. 7}$$

$$V_{min} \le V_{bus,i} \le V_{max}, \quad \text{Eq. 8} \qquad \theta_{ref} = 0. \quad \text{Eq. 9}$$

Eq. 3 represents the power flow equations as described in [8] and [9]. The remaining constraints refer to the active and reactive power limits of the generators (Eq. 4 and Eq. 6), the voltage limits of the nodes (Eq. 8) and the line thermal limits, expressed as constraints on the current (Eq. 5 and Eq. 7). Eq. 9 is added, defining the slack bus, where the phase angle is set to zero.

3.2. VSC-HVDC Modelling and Additional Constraints

A VSC-HVDC system consists of two voltage-source converters, connected either Back-to-Back (BtB) or through a common DC-link. The modelling of the VSC-HVDC line for the OPF calculations, as shown in Figure 1, is based on [3]. The two HVDC converters are represented by AC voltage sources, which are connected to the AC side through the coupling transformer's impedance Z_C. The DC-side is described by the relationships Eq. 10 – Eq. 16. M_{C_i} stands for the PWM amplitude modulation index, V_{DC_i} is the average DC capacitor voltage at the DC side, and R_{DC} the DC cable resistance. From Figure 1 it is evident that for every new HVDC line we incorporate in our system, we need to create two new virtual AC nodes, where we connect the equivalent AC voltage sources of the HVDC-link.

The HVDC-Voltage Source converters allow for two independent power control loops: the active power and the reactive power control loop [3]. In the active power control loop, the converter in the one side is set to control the power flow, while the converter at the other side controls the dc voltage. In the reactive power control loop, the two converters can act independently, controlling either the

voltage at the node, or the reactive power. Combining the two control loops, each converter is able to operate in two possible modes, either in the PV or in the PQ control mode. In the PV control mode, the converter controls the active power and the voltage, while in the PQ mode it controls the active and the reactive power. In both cases, if one converter controls the active power, the other will control the dc voltage.

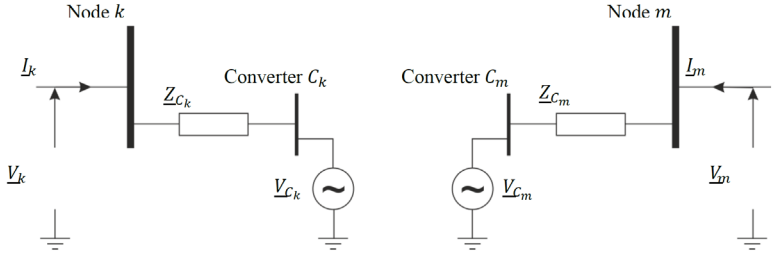

Figure 1: Equivalent circuit of the VSC-HVDC line for OPF calculations

$$Re\{\underline{V}_{C_k}\underline{I}_k^* + \underline{V}_{C_m}\underline{I}_m^*\} + P_{DC}^{loss} = 0 \quad \text{Eq. 10} \qquad V_{C_i} = \frac{M_{C_i}}{2\sqrt{2}} V_{DC_i}, \quad M_{C_i} \in [0,1], \ i = k,m \quad \text{Eq. 11}$$

$$P_{DC}^{loss} = \frac{P_{C_j}^2 R_{DC}}{\left(V_{DC_j}\right)^2} \quad \text{Eq. 12} \qquad \sum V_{DC} = V_{DC_j} - V_{DC_i} + \frac{P_{C_j} R_{DC}}{V_{DC_j}} = 0, \quad i,j = \{k,m\}, i \neq j \quad \text{Eq. 13}$$

$$V_{C_i,min} \leq V_{C_i} \leq V_{C_i,max}, \quad \text{Eq. 14} \qquad V_{DC_i,min} \leq V_{DC_i} \leq V_{DC_i,max}, \quad \text{Eq. 15}$$

$$M_{C_i,min} \leq M_{C_i} \leq M_{C_i,max}, \quad \text{Eq. 16}$$

4. Security-Constrained Optimal Power Flow

In this paper we will focus mainly on the line outages and their effects on the line flows (including the HVDC links). Incorporating the N-1 security criterion means that additional constraints should be introduced, calculating the line loadings when an unplanned outage of a single transmission line occurs. The objective is to find a least cost generation dispatch such that an outage of an arbitrary line will not lead to overloads at any point in the system.

For the implementation of an SC-OPF different approaches exist. Usually, a standard OPF is solved, followed by a contingency analysis which determines the critical overloads. Then these constraints are added to the initial OPF problem and the OPF is solved again [10]. Another possibility is to rely on linear approximations, as in [10] and [6]. An approach suggested in [11] and [9], introduces a second set of power flow equations and constraints, in order to incorporate "critical" conditions associated with the maximum loading margin. In this way, the N-1 criterion is being considered by taking into account the overloading, which occurs during the most severe line outage.

In this paper, we use the current injection method, which allows us to compute the line flows after an outage without having to solve a full power flow. The method was first derived in [12] and [13], and enhanced and applied for FACTS devices in [14]. The current paper proposes a further enhancement to the method in order to incorporate the HVDC corrective control actions after a contingency. In Section 4.1 we describe the basic current injection method, and in Sections 4.2 and 4.3 the enhancement for the HVDC lines, and how this is combined with the method for increased accuracy proposed in [14].

4.1. Current Injection Method

The current injection method is able to determine accurately the line currents after an outage through the solution of a linear system of equations, thus avoiding the need of a full power flow calculation. As a result, constraints for the line currents after an outage can be easily incorporated in the optimization problem. Figure 2 illustrates the concept of the current injection method. The left part shows the system state before the outage, while in the middle the situation after the outage is represented. As

shown in the right part of Figure 2, the outage of the line $(l-p)$ can be represented by a pair of injection currents $\underline{I}_{S_l}, \underline{I}_{S_p}$ at the respective nodes, compensating for the current flowing over the line. Essentially, instead of changing the network topology, injection currents eliminate the line flow, thus simulating the line outage.

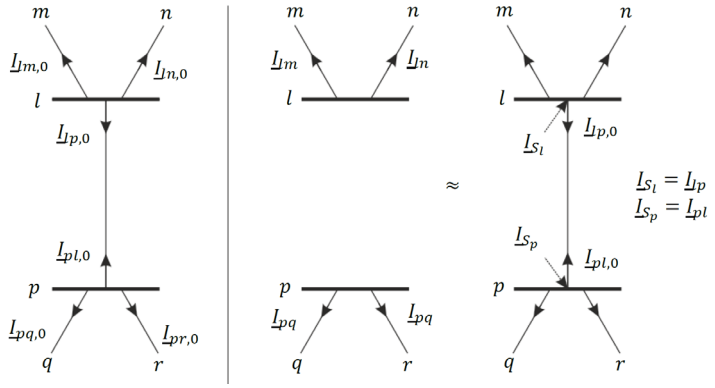

Figure 2: Illustration of the Current-Injection Method

Following the notation in [14], in the non-faulted situation, the relationship between bus voltages and bus currents is given by Eq. 17. $\underline{Z}_0$ is the bus impedance matrix. When a line outage occurs, bus voltages and bus currents change to $\underline{V}_F$ and $\underline{I}_F$ respectively, while the new network topology leads to a new bus impedance matrix $\underline{Z}_F$. Eq. 18 holds in this case.

$$\underline{V}_0 = \underline{Z}_0 \cdot \underline{I}_0, \qquad \text{Eq. 17} \qquad\qquad \underline{V}_F = \underline{Z}_F \cdot \underline{I}_F \qquad \text{Eq. 18}$$

Here, we introduce the vector of injection currents $\underline{I}_S$. Assuming a non-faulted network topology, as given by $\underline{Z}_0$, the injection currents should compensate for the flows on the outaged line. The only non-zero elements of the vector $\underline{I}_S$ correspond to the nodes $\{l, p\}$, where the outage occurred. Hence, Eq. 19 is equivalent to Eq. 18:

$$\underline{V}_F = \underline{Z}_0 \cdot \left(\underline{I}_F + \underline{I}_S\right). \qquad \text{Eq. 19}$$

As a result, the change in the bus voltages after the fault is given by:

$$\Delta\underline{V} = \underline{V}_0 - \underline{V}_F = \underline{Z}_0 \cdot \left(\underbrace{\underline{I}_0 - \underline{I}_F}_{=0} - \underline{I}_S\right). \qquad \text{Eq. 20}$$

As implied by Eq. 20, the basic current injection method assumes that the difference in the bus currents before and after the outage is negligible. Hence, the changes in the line flows can be computed through Eq. 21:

$$\Delta\underline{I}_{line} = \underline{Y}_L \cdot \Delta\underline{V} = \underbrace{-\underline{Y}_L \cdot \underline{Z}_0}_{=\underline{D}} \cdot \underline{I}_S = \underline{D} \cdot \underline{I}_S. \qquad \text{Eq. 21}$$

Here, $\underline{Y}_L$ is the line admittance matrix of the situation without outage. Matrix $\underline{D} = -\underline{Y}_L \cdot \underline{Z}_0$ is known as the matrix of distribution factors [12], reflecting the influence of the injection currents to the line currents.

The injection currents that we calculate have an effect not only on the rest of the line flows but also on the outaged line itself, in a recursive way. In other words, any additional current injection at the nodes l, p will also change the line flow to $\underline{I}_{lp,new} = \underline{I}_{lp,0} - \Delta\underline{I}_{lp}$. As a result, if we wish to eliminate the line flows on the outaged line, the injection currents should be determined from the following equations:

$$\underline{I}_{S_l} = \underline{I}_{lp,0} - \Delta\underline{I}_{lp} = \underline{I}_{lp,0} - \underline{D}_{lp,l} \cdot \underline{I}_{S_l} - \underline{D}_{lp,p} \cdot \underline{I}_{S_p}, \qquad \text{Eq. 22}$$

$$\underline{I}_{S_p} = \underline{I}_{pl,0} - \Delta\underline{I}_{pl} = \underline{I}_{pl,0} - \underline{D}_{pl,l} \cdot \underline{I}_{S_l} - \underline{D}_{pl,p} \cdot \underline{I}_{S_p}, \qquad \text{Eq. 23}$$

where $\Delta\underline{I}_{lp}$ corresponds to the element associated with the line $l-p$ in the vector $\Delta\underline{I}_{line}$, while $\underline{I}_{lp,0}$ is the current that flows on the line before the outage. The notation $\underline{D}_{lp,l}$ indicates the element in the row associated with line $l-p$ and in column p of matrix $\underline{D}$. Using the values for $\underline{I}_{S_l}$ and $\underline{I}_{S_p}$ calculated

through the above equations, the changes in voltages and line currents after the outage can consequently be calculated with the help of Eq. 20 and Eq. 21.

4.2. Inclusion of HVDC lines in the Security-Constrained OPF

As it is evident from Eq. 20, the changes in the bus currents before and after the outage are considered negligible in the basic current injection method. However, as we want to account for the post-contingency control capabilities of the HVDC lines, and based on the HVDC modeling approach in Section 3.2, the bus currents at the nodes where the HVDC line is connected cannot be considered constant. Therefore, we introduce an additional current injection vector, so that the bus currents after the fault to be equal to:

$$\underline{I}_F = \underline{I}_0 + \underline{I}_T. \qquad \text{Eq. 24}$$

The vector $\underline{I}_T$ has non-zero values only at the elements which correspond to the converter nodes of the HVDC line, i.e. nodes C_k and C_m in Figure 1. Consequently, Eq. 20 changes to:

$$\Delta\underline{V} = \underline{V}_0 - \underline{V}_F = -\underline{Z}_0 \cdot \left(\underline{I}_S + \underline{I}_T\right). \qquad \text{Eq. 25}$$

The additional currents have also an effect on the calculation of the injection currents $\underline{I}_{S_l}$ and $\underline{I}_{S_p}$. Eq. 22 and Eq. 23 change to:

$$\underline{I}_{S_l} = \underline{I}_{lp,0} - \underline{D}_{lp,l} \cdot \underline{I}_{S_l} - \underline{D}_{lp,p} \cdot \underline{I}_{S_p} - \underline{D}_{lp} \cdot \underline{I}_T \qquad \text{Eq. 26}$$

$$\underline{I}_{S_l} = \underline{I}_{lp,0} - \underline{D}_{pl,l} \cdot \underline{I}_{S_l} - \underline{D}_{pl,p} \cdot \underline{I}_{S_p} - \underline{D}_{pl} \cdot \underline{I}_T \qquad \text{Eq. 27}$$

In the post-contingency state, we need both HVDC converters to operate under a PV control mode in order to accomplish two functions. First, they should keep the voltage constant to a specified value at both line ends. Second, they must control the active power flowing through the HVDC line in an appropriate way, in order to relieve AC lines from possible overloadings. Eq. 28 refers to the voltage constraints, while Eq. 29 – Eq. 31 express the constraints for active power. In Eq. 28 – Eq. 31, an index i to a matrix refers to a whole row, while an index i to a vector refers to a single element.

$$\begin{aligned}
&\left|\underline{V}_{F_i}\right| = \left|\underline{Z}_{F_i} \cdot \left(\underline{I}_0 + \underline{I}_T\right)\right| = \left|\underline{V}_{i,spec}\right| \qquad \Rightarrow \\
&\left|\underline{V}_{F_i}\right|^2 = \left[\underline{Z}_{F_i} \cdot \left(\underline{I}_0 + \underline{I}_T\right)\right]\left[\underline{Z}_{F_i} \cdot \left(\underline{I}_0 + \underline{I}_T\right)\right]^* = \\
&\quad = \left|\underline{Z}_{F_i} \cdot \underline{I}_0\right|^2 + \left(\underline{Z}_{F_i} \cdot \underline{I}_0\right)\left(\underline{Z}_{F_i} \cdot \underline{I}_T\right)^* + \left(\underline{Z}_{F_i} \cdot \underline{I}_0\right)^*\left(\underline{Z}_{F_i} \cdot \underline{I}_T\right) + \underbrace{\left|\underline{Z}_{F_i} \cdot \underline{I}_T\right|^2}_{neglected} = \left|\underline{V}_{i,spec}\right|^2.
\end{aligned} \qquad \text{Eq. 28}$$

Here, it should be noted that while Eq. 28 refers to the nodes k, m of the AC system, Eq. 29 – Eq. 31 refer to the 'virtual' converter nodes C_k and C_m.

$$\begin{aligned}
P_{C_i,PCC} &= Re\left\{\underline{V}_{F_{C_i}} \cdot \left(\underline{I}_{0_{C_i}} + \underline{I}_{T_{C_i}}\right)^*\right\} = Re\left\{\underline{Z}_{F_{C_i}} \cdot \left(\underline{I}_0 + \underline{I}_T\right) \cdot \left(\underline{I}_{0_{C_i}} + \underline{I}_{T_{C_i}}\right)^*\right\} \\
&= Re\left\{\left(\underline{Z}_{F_{C_i}} \cdot \underline{I}_0\right) \cdot \underline{I}_{0_{C_i}}{}^* + \left(\underline{Z}_{F_{C_i}} \cdot \underline{I}_0\right) \cdot \underline{I}_{T_{C_i}}{}^* + \left(\underline{Z}_{F_{C_i}} \cdot \underline{I}_T\right) \cdot \underline{I}_{0_i}{}^* + \underbrace{\left(\underline{Z}_{F_{C_i}} \cdot \underline{I}_T\right) \cdot \underline{I}_{T_{C_i}}{}^*}_{neglected}\right\}.
\end{aligned} \qquad \text{Eq. 29}$$

In Eq. 28 – Eq. 29, we neglect the values of the terms where the injection currents appear squared, as they are comparably low. The elements of the $\underline{I}_T$ vector, not corresponding to a converter should be set to zero.

Equivalently to Eq. 10 for the non-faulted state, Eq. 30 requires that the change in the active power flow after the fault must also be balanced. Here, the effect of the DC line losses, which have a comparably small contribution, is neglected. As implied by Eq. 29 and Eq. 30, an additional optimization variable $P_{C_k,PCC}$ is added to the optimization problem for each considered outage, bounded through Eq. 31.

$$P_{C_k,PCC} = -P_{C_m,PCC} \qquad \text{Eq. 30}$$

$$-P_{HVDC,limit} \leq P_{C_k,PCC} \leq P_{HVDC,limit} \qquad \text{Eq. 31}$$

Hence, splitting the equation system Eq. 26 – Eq. 29 into real and imaginary parts, and forming the linear system of Eq. 32, the currents $\underline{I}_S$ and $\underline{I}_T$ can be determined. Here, A_{ic} is derived directly from the linear terms, while b_{ic} from the constant terms of Eq. 26 – Eq. 29. Subsequently, the new line

currents in the faulted case can be determined through Eq. 33. The entries in $\underline{I}_{line}$ that correspond to the outaged line in both directions are equal to the virtual currents which are eliminated from the injection currents $\underline{I}_S$. Thus, for correctness these entries should be set to zero.

$$A_{ic}\begin{pmatrix} Re\{\underline{I}_S\} \\ Im\{\underline{I}_S\} \\ Re\{\underline{I}_T\} \\ Im\{\underline{I}_T\} \end{pmatrix} = b_{ic}, \quad \text{Eq. 32} \qquad \underline{I}_{line} = \underline{I}_{line,0} - \Delta\underline{I}_{line} = \underline{I}_{line,0} + \underline{Y}_L \cdot \underline{Z}_0 \cdot (\underline{I}_S + \underline{I}_T) \quad \text{Eq. 33}$$

4.3. Extension of the Basic Current Injection Method for Increased Accuracy

In [14] an extension to the current injection method was proposed in order to improve its accuracy. The reasoning lies on the fact that the bus currents do change after the fault. The authors distinguish between the three different types of buses and form the equations, which are restated here, in Eq. 34 – Eq. 39, for the sake of completeness. The vector $\underline{I}_S$ has, again, non-zero values only at the nodes of the outaged line. On the other hand, due to the extension, the only zero elements of the vector $\underline{I}_T$ are the ones corresponding to PQ buses without loads. For the slack bus, Eq. 34 should be satisfied, while for the PV buses, Eq. 36 and Eq. 35 should be fulfilled. Finally, Eq. 35 and Eq. 37 should hold for PQ buses. For further details the interested reader can refer to [14].

$$\Delta\underline{V}_i = -\underline{Z}_0 \cdot (\underline{I}_S + \underline{I}_T) = 0 \quad \text{Eq. 34} \qquad P_i = Re\{\underline{V}_{F_i} \cdot (\underline{I}_{0_i} + \underline{I}_{T_i})^*\} \quad \text{Eq. 35}$$

$$|\underline{V}_{F_i}| = |\underline{Z}_F \cdot (\underline{I}_0 + \underline{I}_T)| = |\underline{V}_{0_i}| \quad \text{Eq. 36} \qquad Q_i = Im\{\underline{V}_{F_i} \cdot (\underline{I}_{0_i} + \underline{I}_{T_i})^*\} \quad \text{Eq. 37}$$

Due to the extension, the HVDC converters are not bound any more to operate in PV control mode, but we can rather distinguish between two alternatives. If the HVDC converter is connected to a PQ bus, then it should operate in a PV mode, in order to keep the post-fault bus voltage to the specified value. If, however, the converter is connected to a PV bus, then the voltage will be kept steady from the voltage controller (e.g. AVR of a generator) that is connected at that bus. Thus, the converter can operate in a PQ control mode with the objective to keep the reactive power injection/withdrawal steady at the pre-fault level. The formulation of such a constraint is similar to Eq. 37. Since operating in a PV control mode after an outage usually requires the injection of reactive power, thus limiting the active power transfer capability of the HVDC converter, a PQ control mode could allow an increased active power transfer.

5. Case Studies

For the first two case studies we used the 10-bus power system depicted in Figure 3. The system is similar to the one used in [8] and [6]. It emulates to a certain extent the interconnecting flows between Switzerland, France and Italy. The system data and main characteristics can be found in [6].

In the following case studies, the post-fault line flow computations from the current injection method are compared with the results from an AC power flow (AC-PF). Since the HVDC active and reactive power setpoints have already been determined from the OPF at both system and converter nodes, and the AC-PF serves only for comparison purposes, the simplified steady-state model of the HVDC can be used for the AC-PF [2]. Therefore, each converter is modeled as a generator, as already shown in Figure 1. The virtual converter buses are assigned to be PQ buses. For the SC-OPF the SNOPT Solver from Tomlab Optimization (www.tomopt.com) was used.

5.1. Case Study #1

In this case study we place the HVDC line between nodes 6 and 7, replacing the existing AC interconnection between France and Italy. Node 6 is a PQ bus, while Node 7 is a PV bus, thus allowing the study of different control modes for the converters. The capacity of the converters is set to 3000 MVA. We assume that a transfer of 1700 MW has already been agreed from node 6 to node 7, through e.g. a day-ahead market clearing. The voltages at both ends of the line are set to 1.0 p.u.

during normal operation. The goal of this case study is to examine in what extent the HVDC line can contribute to congestion relief in case of the most critical contingency, which is the outage of line 2-9.

Different corrective control strategies can be envisioned. Here, we set the post-contingency voltage level of PV-controlled converter (node 6) equal to 1.05 p.u., while the active power is allowed to vary in order to relieve any overloadings. The PV-buses should keep their pre-fault voltage levels.

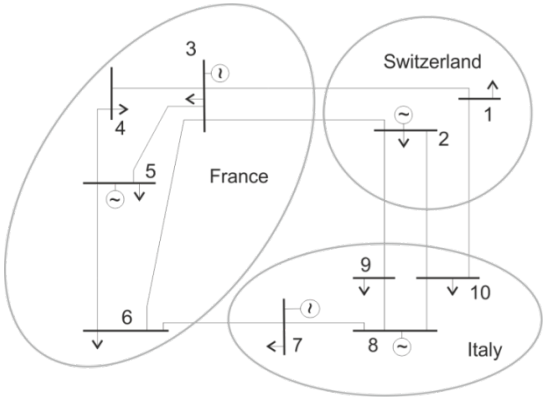

VSC-HVDC:

- Replacing line 6-7 in Case Study #1
- Replacing line 1-10 in Case Study #2

$M_{C_i,min} = 0.85$ $M_{C_i,max} = 1.00$

$R_{DC} = 0.00334$ p.u. $V_{DC_m} = 3.3$ p.u.

$Z_{C_i} = 0.001 + j0.01$ p.u.

Emergency Overload Rating:

$$I_{ij,max}^{emg} = 1.2 \cdot I_{ij,max}$$

Due to generator costs differences and loads, the power flow in the network is generally from the top left towards the bottom right.

Figure 3: 10-bus network used for the simulations in the first two case studies

As shown in Figure 4, the voltage at node 6 indeed increases from 1.0 p.u. and reaches the value of 1.058 p.u. The voltages at the PV buses remain at the same levels. Bus 9, which is a PQ bus where the outaged line was connected, experiences a significant voltage drop. The post-contingency flow over the HVDC line is determined equal to 2955.7 MW, flowing from node 6 to node 7. In Figure 5, the accuracy of the current injection method is examined. As shown, the post-contingency line loadings are approximated sufficiently well. For line 2-10, which is the critical line loading, the error is 2.7%.

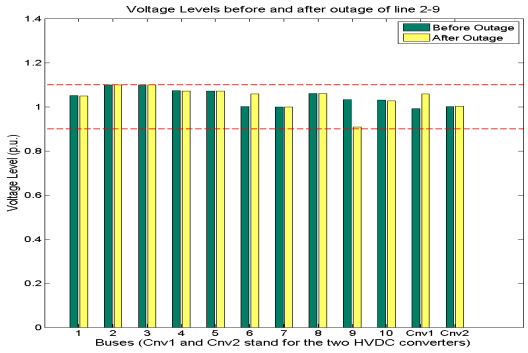

Figure 4: Voltage levels before and after the outage of line 2-9. The voltage at node 6 increases after the contingency.

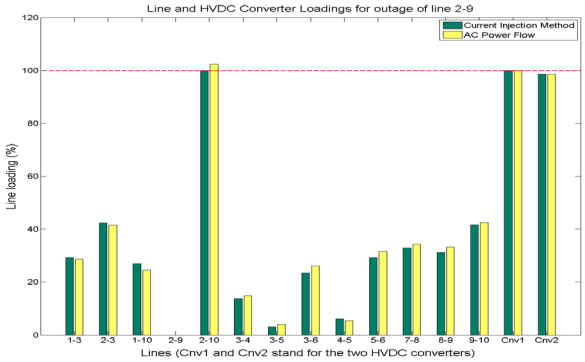

Figure 5: Comparison of the line loadings from Current Injection with the line loadings determined through an AC power flow.

5.2. Case Study #2

In this case study we allow the SC-OPF to determine the optimal voltage values and power dispatch, both in pre- and post-fault case, in order to achieve the minimum costs. Here, the HVDC line replaces the AC line connecting nodes 1 and 10, with a converter capacity of 2000 MVA. Additionally, in order to study the performance of the algorithm, and more specifically the inverse of the HVDC flow after a contingency, we exchange the loads at buses 1 and 10, i.e. L_{10} is now at bus 1 and vice-versa. Critical contingency in this case is considered the outage of line 6-7.

In Table I, the total generation costs from a Standard AC-OPF dispatch and from the SC-OPF dispatch both with and without post-contingency control (PCC) of the HVDC line are shown. We observe that the 'Cost of Security', i.e. the additional costs in order to guarantee the N-1 security, can significantly decrease if we take advantage of HVDC PCC capabilities. In Table II, the active and reactive power

setpoints of the HVDC line are presented. Observe here, that after the fault, the HVDC active power changes direction, flowing from node 1 to node 10.

Table I: Total Generation Costs resulting from a Standard AC-OPF dispatch and from a SC-OPF dispatch with and without PCC of HVDC. (Critical Contingency: outage of line 6-7).

Standard OPF	*SC-OPF without PCC*	*SC-OPF with PCC*
315'442 €/h	324'816 €/h	316'328 €/h
Cost of Security	9'374 €/h	886 €/h

Table II: HVDC active and reactive power setpoints resulting from a Standard AC-OPF, and from the SC-OPF with PCC during the pre-fault and post-fault state (P_{HVDC} positive direction: 1→10). Values are in MW resp. MVAr.

	Standard OPF	*SC-OPF (pre-fault dispatch)*	*SC-OPF (PCC of HVDC)*
P_{HVDC}	568.8	-192.3	1400.1
Q_{conv1}	731.1	284.8	1428.2
Q_{conv2}	320.1	-96.7	-271.0

As shown in Figure 6, the post-contingency line loadings are approximated, again, sufficiently well. For line 2-10, which is the most critical line loading, the error is 2.6%. Figure 7 refers exclusively to the SC-OPF solution where the PCC capabilities are enabled. The line loadings during three different states are presented: (a) pre-fault state (no outage), (b) outage of line 6-7 but HVDC setpoints same as in pre-fault state (no PCC), and (c) outage of line 6-7 and post-contingency control of HVDC line. We observe that if no post-contingency control takes place, line 2-10 exceeds its emergency overload rating.

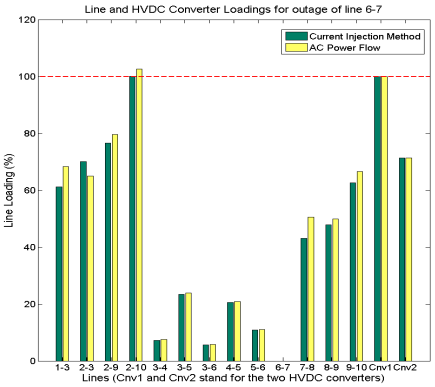

Figure 6: Comparison of the line loadings from Current Injection with the line loadings determined through AC-PF.

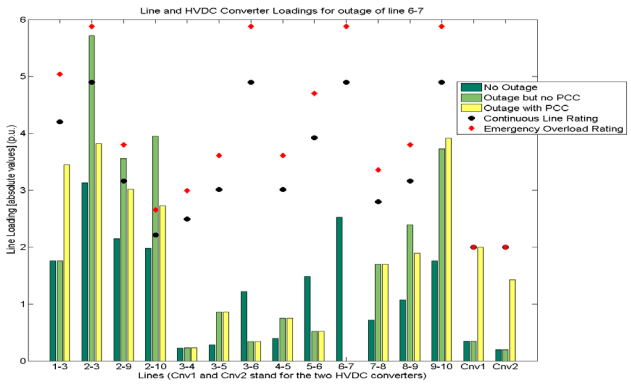

Figure 7: Comparison of Line Loadings during (a) pre-fault state, (b) post-fault state but with no post-contingency control (HVDC setpoints same as in the pre-fault state), and (c) post-fault state with HVDC post-contingency control. The HVDC converters have no overload capability.

5.3. Case Study #3: the European Network

The EU Project IRENE-40 (www.irene-40.eu) aims to identify the appropriate transmission expansion measures in order to achieve a more secure, sustainable, and economically competitive European power system. Within this context, simulations based on different future generation scenarios are carried out. With respect to security, the objective is to identify the appropriate reinforcements in order to minimize the 'cost of security'. Hourly generation and load data for the years 2010, 2020, 2030, 2040, and 2050 are provided for each EU-27 member state, Norway, and Switzerland [15].

Here, we study a single-hour snapshot of the year 2050. The generation and load data are taken from the scenario RES, which projects a high share of renewable generation in Europe (~80%) by the year 2050. In a future work, detailed results will be published concerning the appropriate expansion measures for each scenario. In this paper, the focus is on the description of the algorithm and its performance. For illustration purposes, we compare the case where no expansion measures are undertaken (i.e. system as in 2010) and the case where one AC and three HVDC lines are added. The additional HVDC lines connect UK with the Netherlands (BritNed), Norway with Germany (NorGer), and Sweden with Lithuania (NordBalt). The lines are already in construction/planning phase and are based on the LCC-HVDC technology. In order to test the performance of the algorithm, we assume they are VSC-HVDC lines. The AC line connects Lithuania with Poland. The studies are carried out

with a single-node per country model, comprising 32 nodes and 104 branches. Each interconnection (except for the submarine cables) is modeled as two identical AC lines. Thus, a line outage will result to a loss of only 50% of the interconnection capacity. The line data are aggregations of real data provided by UCTE (now ENTSO-E) (www.entsoe.eu).

Figure 8 presents the line loadings after the expansion, resulting from a Standard OPF dispatch and the SC-OPF. For the SC-OPF, the twelve most critical contingencies are taken into account. As shown in Table III, the expansion results to a reduction of about 6.4% to the 'Cost of Security' for this snapshot.

Table III: Cost of Security calculations when no transmission expansion takes place, and after the addition of one AC line (LT-PL) and three HVDC lines (NL-UK, DE-NO, LT-SE). The SC-OPF takes into account the 12 most critical line outages.

	No Expansion	*Addition of 1 AC + 3 HVDC lines*
Standard OPF	9.52 million €/h	9.50 million €/h
SC-OPF with PCC	10.61 million €/h	10.52 million €/h
Cost of Security	1.09 million €/h	1.02 million €/h
Reduction in Cost of Security	6.4%	

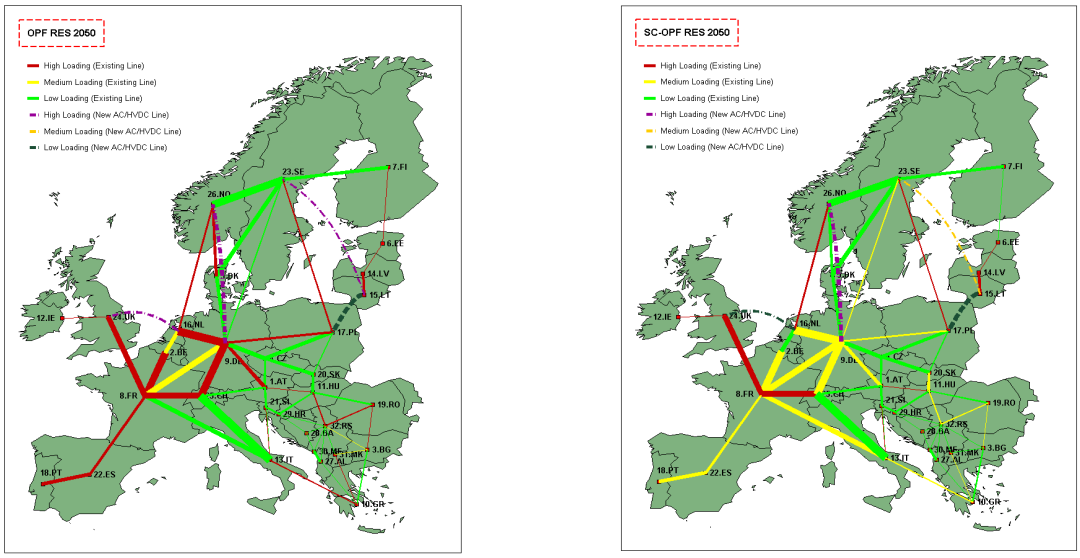

Figure 8: Line Loadings during a Standard OPF and the SC-OPF dispatch. Both illustrations correspond to the 3HVDC+1AC expansion case. The line width is proportional to the Net Transfer Capacity of the interconnection. Loadings: High >70%, Medium 50-70%, Low <50%.

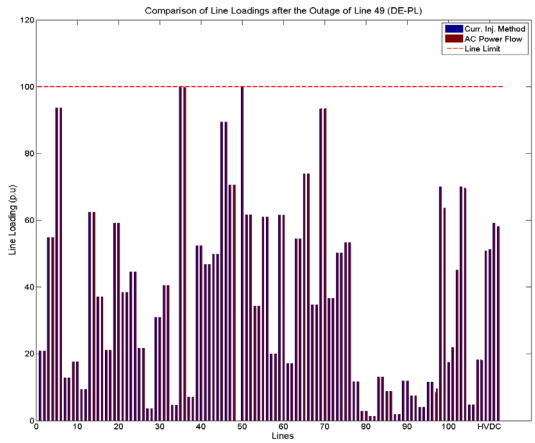

Figure 9: Comparison of the derived line loadings from the current injection method with the line loadings determined through an AC-PF, during the outage of line DE-PL.

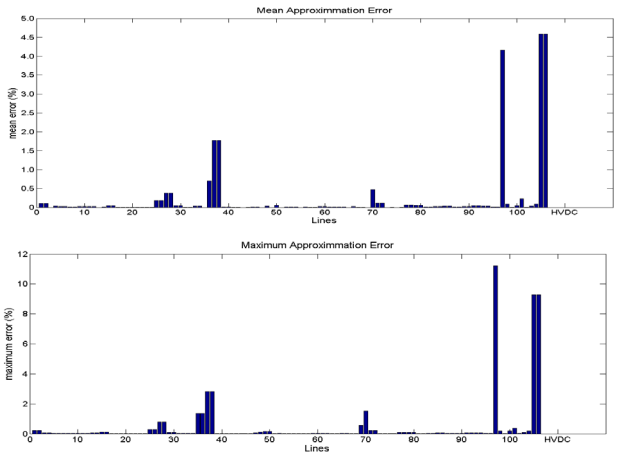

Figure 10: Mean and maximum error of the line loadings derived from the current injection method for the 12 critical contingencies.

Figure 9 presents the line loadings resulting from the current injection method and from an AC power flow during the outage of line DE-PL, one of the critical contingencies considered. As it is shown, the

line loadings are well approximated. In Figure 10, the mean and maximum error of the line loadings for the twelve critical contingencies is presented. It can be observed that the mean error for most lines is close to zero, while in any case it does not exceed 5%. For most lines, the maximum error is also near zero. In only a few cases it reaches a value of 8-11%. The results are in line with the results presented in [14].

In Table IV, the active and reactive power setpoints for all three HVDC lines, during a Standard OPF and an SC-OPF in the pre-fault state are presented. Indicatively, the post-fault cases of lines DE-PL and IT-SI outages are also shown.

Table IV: HVDC active and reactive power setpoints resulting from a Standard AC-OPF, and from the SC-OPF with PCC during the pre-fault and post-fault state (for Line Outages 49: DE-PL and 65: IT-SI). All values are in MW resp. MVAr. Arrow (e.g. NL→UK) shows the positive direction of the power flow.

	BritNed (UK→NL)			NorGer (NO→DE)			NordBalt (SE→LT)		
	P_{HVDC}	Q_{conv1}	Q_{conv2}	P_{HVDC}	Q_{conv1}	Q_{conv2}	P_{HVDC}	Q_{conv1}	Q_{conv2}
OPF	-999.98	5.55	-16.29	1396.76	-25.27	0.23	699.19	23.46	0.01
SC-OPF	-533.32	-6.49	-10.35	1396.76	-33.31	0.09	413.02	-10.72	2.27
Out. 49	-313.00	-3.84	-7.30	1227.40	-32.15	2.12	699.97	6.15	6.15
Out. 65	-700.00	-5.17	-8.41	1293.85	-32.89	0.80	78.28	11.42	8.00

6. Conclusions

In this paper, a Security-Constrained Optimal Power Flow including post-contingency control of HVDC lines was described. HVDC lines based on the Voltage-Source Converter technology are expected to play a significant role in the future power systems. The algorithm proposed in this paper integrates the control capabilities of the VSC-HVDC technology in a single optimization problem, without the need to solve a detailed power flow or OPF for each contingency. The approach is based on the current injection method and takes full advantage of the VSC-HVDC line flexibility. It allows setting post-contingency voltage setpoints at the HVDC nodes and determines the optimal active HVDC power flow – pre- and post-fault – in order to avoid line overloads. After a contingency, each HVDC converter side can be controlled either in PV or in PQ control mode, depending on the type of nodes it is connected.

The algorithm can be used for both power system operation and planning studies. The term 'Cost of Security' is introduced for planning studies, which provides a quantitative index for evaluating infrastructure reinforcement measures, with respect to power system security.

Three case studies were presented, which examined the performance of the algorithm. It was shown that the current injection method approximates well the post-fault line flows. Furthermore, taking advantage of the HVDC post-contingency control, the second case study showed that a significant decrease in the 'Cost of Security' can be achieved. The third case study presented the application of the algorithm on a power system model which studies the cross-border power flows of the European power system. Multiple HVDC lines and critical contingencies were included in the SC-OPF computation. Results about the 'Cost of Security' and HVDC post-contingency setpoints for a single snapshot were provided. Future work will include the detailed evaluation of different expansion scenarios in the European power system, applying the proposed algorithm and determining the solution which leads to the least 'Cost of Security'.

ACKNOWLEDGEMENTS

The research work described in this paper has been carried out within the scope of the project "Infrastructure Roadmap for Energy Networks in Europe (IRENE-40)", supported under the 7th Framework Programme of the European Union, grant agreement 218903. The authors would like to thank the IRENE Consortium for the provision of a significant amount of the data, necessary for the simulation of Case Study #3.

BIBLIOGRAPHY

[1] M. Henderson, J. Gagnon and D. Bertagnolli, "Planning Issues for HVdc," in *28th IEEE Power Systems Conference and Exhibition (PSCE)*, Atlanta, GA, USA, 2006.

[2] S. Cole, Steady-State and Dynamic Modelling of VSC HVDC Systems for Power System Simulation, PhD

Dissertation, KU Leuven, 2010.

[3] A. Pizano-Martinez, C. R. Fuerte-Esquivel, H. Ambriz-Pérez and E. Acha, "Modeling of VSC-Based HVDC Systems for a Newton-Raphson OPF Algorithm," *IEEE Transactions on Power Systems,* vol. 22, no. 4, pp. 1794-1803, November 2007.

[4] W. Shao and V. Vittal, "LP-Based OPF for Corrective FACTS Control to Relieve Overloads and Voltage Violations," *IEEE Transactions on Power Systems,* vol. 21, no. 4, pp. 1832-1839, November 2006.

[5] A. Lotfjou, M. Shahidehpour and F. Yong, "Hourly Scheduling of DC Transmission Lines in SCUC with Voltage Source Converters," *IEEE Transactions on Power Delivery,* vol. 26, no. 2, pp. 650-660, April 2011.

[6] S. Chatzivasileiadis, T. Krause and G. Andersson, "Flexible AC Transmission Systems (FACTS) and Power System Security - A Valuation Framework," in *Proceedings of the IEEE PES General Meeting*, Detroit, USA, 2011.

[7] ENTSO-E, "Operation Handbook," European Network of Transmission System Operatos for Electricity, 2009.

[8] C. Schaffner, "Valuation of controllable devices in liberalized electricity markets," Ph.D. Dissertation, ETH Zurich, Switzerland, 2004.

[9] R. Zarate-Miñano, A. Conejo and F. Milano, "OPF-based security redispatching including FACTS devices," *Generation, Transmission, Distribution, IET,* vol. 2, no. 6, pp. 821-833, 2008.

[10] R. Christie, B. Wollenberg and I. Wangensteeen, "Transmission management in the deregulated environment," *Proceedings of the IEEE,* vol. 88, no. 2, pp. 170-195, 2000.

[11] F. Milano, C. Canizares and M. Invernizzi, "Multiobjective optimization for pricing system security in electricity markets," *IEEE Transactions on Power Systems,* vol. 18, no. 2, pp. 596-604, 2003.

[12] G. Schnyder and H. Glavitsch, "Integrated Security Control using an Optimal Power Flow and Switching Concepts," *IEEE Transactions on Power Systems,* vol. 3, no. 2, pp. 782-790, May 1988.

[13] R. Bacher and H. Glavitsch, "Network Topology Optimization with Security Constraints," *IEEE Transactions on Power Systems,* vol. 1, no. 4, pp. 103-111, November 1986.

[14] G. Hug-Glanzmann and G. Andersson, "An Accurate and Efficient Current Injection Method for the Determination of the System State during Line Outages," in *16th Power Systems Computation Conference (PSCC)*, Glasgow, 2008.

[15] S. Dijkstra, E. Gaxiola, F. Nieuwenhout, G. Orfanos, O. Ozdemir and A. van der Welle, "European scenario synthesis to be used for electricity transmission network planning," in *9th International Conference on the European Energy Market*, Florence, 2012.